Electronic and Local Structural Properties of the Bi 2 Sr 2 (Ca 1− x Y x)Cu 2 O 8+ δ Family of Materials, Studied by X−ray Absorption Spectroscopy

ARTICLE *in* CHEMISTRY OF MATERIALS · APRIL 2000

Impact Factor: 8.35 · DOI: 10.1021/cm9907007

Electronic and Local Structural Properties of the $Bi_2Sr_2(Ca_{1-x}Y_x)Cu_2O_{8+\delta}$ Family of Materials, Studied by X-ray Absorption Spectroscopy

I-Jui Hsu,[†] Ru−Shi Liu,*[,†] Jin-Ming Chen,[‡] Ru-Gun Liu,[‡] Ling-Yun Jang,[‡] Jyh-Fu Lee,[‡] and Kenneth D. M. Harris[§]

Department of Chemistry, National Taiwan University, Taipei, Taiwan, Republic of China; Synchrotron Radiation Research Center (SRRC), Hsinchu, Taiwan, Republic of China; and School of Chemistry, University of Birmingham, Birmingham, U.K.

Received November 22, 1999

The hole distribution of overdoped, optimum-doped and underdoped states in the series $Bi_2Sr_2(Ca_{1-x}Y_x)Cu_2O_{8+\delta}$ compounds has been investigated by high-resolution O K-edge and Cu L-edge X-ray absorption near-edge-structure (XANES) spectra. Near the O 1s edge, a well-pronounced pre-edge peak with maximum at ∼528.3 eV is found and is ascribed to the excitations of O 1s electron to O 2p hole states located in the CuO_2 planes. The intensity of this pre-edge peak decreases as the Y doping increases, demonstrating that the chemical substitution of Y^{3+} for Ca^{2+} in $Bi_2Sr_2(Ca_{1-x}Y_x)Cu_2O_{8+\delta}$ gives rise to a decrease in hole concentrations within the CuO_2 planes. The results from the Cu L-edge X-ray absorption spectra are consistent with those from O 1s X-ray absorption spectra. The local structure of the pyramidal CuO_5 in $Bi_2Sr_2(Ca_{1-x}Y_x)Cu_2O_{8+\delta}$ has been determined from extended X-ray absorption fine-structure (EXAFS) spectra. It was found that the axial Cu−O bond distances contract and the equatorial Cu−O bond distances expand as the Y content increases. Such results are strongly correlated to a decrease in the hole concentration within the CuO_2 plane, which controls the superconductivity.

Introduction

The occurrence of superconductivity adjacent to a metal−insulator boundary is a characteristic feature of many high-T_c superconducting cuprates, such as $La_{2-x}Sr_xCuO_4$, $YBa_2Cu_3O_{7-\delta}$, $Bi_2Sr_2(Ca_{1-x}Y_x)Cu_2O_{8+\delta}$, and $(Tl_{0.5}Pb_{0.5})Sr_2(Ca_{1-x}Y_x)Cu_2O_7$.[1−4] Up to now, the precise mechanism of high-T_c superconductivity has not been fully understood. However, a system exhibiting a composition-induced metal−superconductor−insulator transition may offer great potential for investigating the important structural and electronic characteristics, which can lead to superconductivity at such high temperatures. One such system is the so-called Bi-2212 system, $Bi_2Sr_2(Ca_{1-x}Y_x)Cu_2O_{8+\delta}$.[5−7] The crystal structure of $Bi_2Sr_2CaCu_2O_{8+\delta}$ can be described in terms of half the unit cell of an intergrowth of triple rock salt-type layers {[BiO][SrO]} with double $[Sr(Ca,Y)Cu_2O_5]$ oxygen deficient perovskite layers as shown in Figure 1. The latter layers are formed by sheets of corner-sharing CuO_5 pyramids interleaved with calcium (Y ions substitute into the Ca sites). The square-pyramidal CuO_5 arrangement between Cu and O is exhibited by $Bi_2Sr_2CaCu_2O_{8+\delta}$. The unit cell of $Bi_2Sr_2CaCu_2O_{8+\delta}$ is orthorhombic, and it has two independent Cu−O bonds [denoted by Cu−O(1) and Cu−O(2)] within the CuO_2 planes and one Cu−O bond [denoted by Cu−O(3)] in the apical direction. A relatively sharp metal−insulator transition takes place at $x \sim 0.5$, giving rise to antiferromagnetic order. The normal-state resistivity increases systematically with increasing Y concentration, implying a decreased number of charge carriers consistent with reported Hall effect measurements.[8,9] The depression of T_c and the decreasing carrier concentration have been interpreted as a result of hole filling due to the additional electrons contributed by the trivalent Y^{3+} ion relative to the divalent Ca^{2+} ion.

It has been demonstrated experimentally that hole states play an important role for superconductivity in p-type cuprate materials. Therefore, knowledge of the unoccupied electronic structure near the Fermi level of these compounds is a crucial step toward deriving a comprehensive understanding of the mechanism of superconductivity. The X-ray absorption spectra are determined by electronic transitions from a selected atomic core level to the unoccupied electronic states near

[†] National Taiwan University.
[‡] Synchrotron Radiation Research Center.
[§] University of Birmingham.

(1) Torrance, J. B.; Bezinge. A.; Nazzal. A. I.; Huang, T. C.; Parkin, S. S. P.; Keane, D. T.; LaPlaca, S. J.; Horn, P. M.; Held G. A. *Phys. Rev. B.* **1989**, *40*, 8872.
(2) Tokura, Y.; Torrance, J. B.; Huang, T. C.; Nazzal, A. I. *Phys. Rev. B.* **1988**, *38*, 7156.
(3) Ruscher, C. H.; Gottek, M.; Schmidt, B.; Quitmann, C.; Guntherodt, G. *Physica C* **1992**, *204*, 30.
(4) Liu, R. S.; Edwards, P. P.; Huang, Y. T.; Wu, S. F.; Wu, P. T. *J. Solid State Chem.* **1990**, *86*, 334.
(5) Manthiram. A.; Goodenough, J. B. *Appl. Phys. Lett.* **1988**, *53*, 420.
(6) Tamegai, T.; Koga, K.; Suzuki, K.; Ichihara, M.; Sakai, F.; Iye, Y. *Jpn. J. Appl. Phys.* **1989**, *28*, l112.
(7) Mazaki, H.; Kakihana, M.; Yasuoka, H. *Jpn. J. Appl. Phys.* **1991**, *30*, 38.
(8) Maeda, A.; Hase, M.; Tsukada, T.; Noda, K.; Takebayashi, S.; Uchinokura, K. *Phys. Rev. B* **1990**, *41*, 6418.
(9) Groen, W. A.; de Leeuw, D. M.; Feiner, L. F. *Physica C* **1990**, *165*, 55.

10.1021/cm9907007 CCC: $19.00
Published on Web 03/25/2000

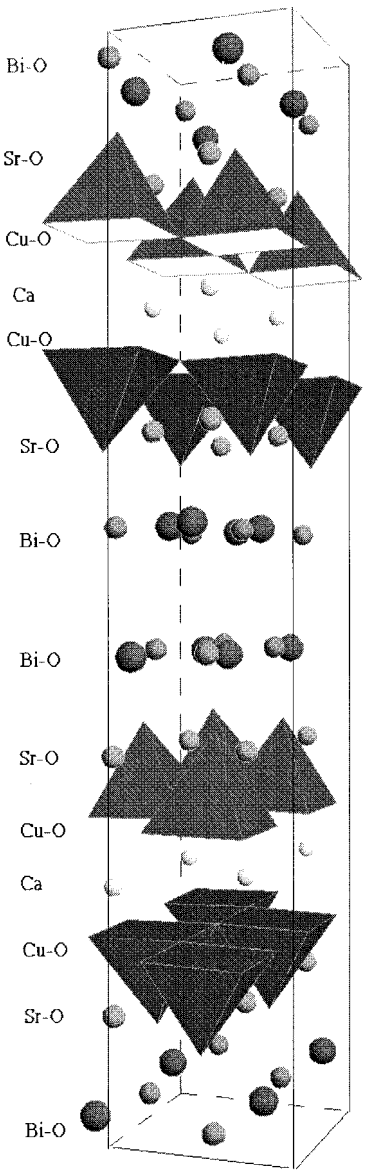

Figure 1. Idealized crystal structure of $Bi_2Sr_2CaCu_2O_{8+\delta}$.

the Fermi level. X-ray absorption near edge structure (XANES) is therefore a direct probe of the character and local density of hole states responsible for high-T_c superconductivity. Mante et al.[10] and Tjernberg et al.[11] have demonstrated that a pronounced pre-edge peak at 528.5 eV corresponding to holes in the singlet band formed on p-type doping decreases continuously as the Y content in $Bi_2Sr_2(Ca_{1-x}Y_x)Cu_2O_{8+\delta}$ (measured by electron energy-loss spectroscopy) increases. Moreover, the extended X-ray absorption fine structure (EXAFS) technique has the advantage of directly observing the local structure around the specific atoms. Kim et al.[12] have assumed that one Cu atom was coordinated with four oxygen atoms in $Bi_2Sr_2(Ca_{1-x}Y_x)Cu_2O_{8+\delta}$ to explain the Cu K-edge XANES and EXAFS results. They showed the average Cu−O bond distance to increase upon the substitution of Y. However, one Cu atom is actually coordinated with five oxygen atoms in $Bi_2Sr_2(Ca_{1-x}Y_x)Cu_2O_{8+\delta}$ (as shown in Figure 1). Moreover, Choy et al.[13] have applied both XANES and EXAFS methods to find that for materials of the type $(HgX_2)_{0.5}Bi_2Sr_2CaCu_2O_y$ (X = Br and I) the charge transfer between the host ($Bi_2Sr_2CaCu_2O_y$) and guest (HgX_2) is mainly responsible for the T_c evolution upon intercalation. The values of T_c for these compounds must be related to the variation of hole concentration rather than electronic coupling along the *c*-axis.

In the present paper, an attempt has been made to combine XANES and EXAFS in a complementary manner to provide not only electronic structural information concerning the copper and oxygen ions but also local structural information concerning the neighboring atoms of the copper ions across the $Bi_2Sr_2(Ca_{1-x}Y_x)Cu_2O_{8+\delta}$ system. The results reported here may be able to stimulate further experiments and theories, since the system studied offers a remarkable opportunity for testing and evaluating theories of high-T_c superconductivity.

Experimental Section

Sample Preparation. Polycrystalline samples of $Bi_2Sr_2(Ca_{1-x}Y_x)Cu_2O_{8+\delta}$ with Y content in the range $0.0 \le x \le 1.0$ were synthesized by conventional solid-state reactions as follows. At first, the powder reagents Bi_2O_3, $SrCO_3$, $CaCO_3$, CuO, and Y_2O_3 were mixed with a molar ratio Bi:Sr:Ca:Y:Cu = 2:1:1 − *x*:*x*:2. Then, the powders were calcined at 816 °C for 16 h and 840 °C for 10 h in air. For $x = 0.0$, the prefired material was calcined again at 870 °C for 90 h with intermittent grindings. After that, the powders were pressed into 1 cm disk-shaped pellets with 2 ton/cm^2 pressure and finally sintered at 870 °C for 50 h in air. For the compounds with $x = 0.1-1.0$, the prefired powders were calcined at 870 °C for 30 h and 880 °C for 10 h with intermittent grinding. After that, the powders were pressed into disk-shaped pellets and sintered at 890 °C for 10 h in air.

Characterization. Structural properties and phase purity were characterized by powder X-ray diffraction (XRD). The powder X-ray diffraction data were collected with a step-scan procedure on a Scintag-X1-type diffractometer using Cu Kα radiation and a Peltier [Si(Li)]-cooled solid-state detector. Each diffraction pattern was calibrated using α-quartz as an external standard. The superconducting transition temperature was determined by zero-field-cooled susceptibility measurements with a Quantum Design SQUID magnetometer. To avoid intergranular effects, all samples were ground to powders.

X-ray Absorption Measurements. All X-ray absorption experiments were carried out at the Synchrotron Radiation Research Center (SRRC), Hsinchu, Taiwan. All measurements were made at room temperature.

The XANES measurements at the O K-edge and Cu L_{23} edge were performed at the 6-m high-energy spherical grating monochromator (HSGM) beamline. All samples were pressed into pellets, attached by conducting tape, and then put into an ultrahigh vacuum chamber (10^{-9} Torr) in order to avoid surface contamination. The X-ray−fluorescence yield spectra were recorded with a microchannel plate (MCP) detector, consisting of a dual set of MCPs with an electrically isolated grid mounted in front. For X-ray−fluorescence yield detection, the grid was set to a voltage of 100 V while the front of the MCPs was set to −2000 V and the rear to −200 V. The grid bias ensured that positive ions would not be detected while the MCP bias ensured that no electrons were detected. The

(10) Mante, G.; Schmalz, Th.; Manzke, R.; Skibowski, M.; Alexander, M.; Fink, J. *Surf. Sci.* **1992**, *269/270*, 1071.
(11) Tjernberg, O.; Nylen, H.; Chiaia, G.; Soderholm, S.; Karlsson, U. O.; Qvarford, M.; Lindau, I.; Puglia, C.; Martensson, N.; Leonyuk, L. *Phys. Rev. Lett.* **1997**, *79*, 499.
(12) Kim, D. K.; Choy, J. H.; Osada, M.; Kakihana, M.; Yoshimura, M. *Solid State Ionics* **1998**, *108*, 291.
(13) Choy, J. H.; Hwang, S. J.; Park, N. G. *J. Am. Chem. Soc.* **1997**, *119*, 1624.

MCP detector was located ~2 cm from the sample and oriented parallel to the sample surface. Photons were incident at an angle of 45° with respect to the sample normal. The incident photon flux (I_0) was monitored simultaneously by a Ni mesh located after the exit slit of the monochromator. All X-ray absorption spectra were normalized to I_0. The photon energies were calibrated within an accuracy of ~0.1 eV using the known O K-edge and Cu L -edge absorption peaks of CuO. The energy resolution of the monochromator was set to ~0.22 eV for the O K-edge absorption measurements.

The EXAFS measurements were performed in transmission mode at the S-5B/W20 X-ray Wiggler beamline with a double-crystal Si (111) monochromator. The higher X-ray harmonics were minimized by detuning the double-crystal monochromator to 80% of the maximum. It is important that the size[14] of the particles should be smaller than one absorption length in the material, $\mu d < 1$, where d is the particle size and μ is the total absorption coefficient. Thus, all samples in this EXAFS experiment were finely ground and sieved through 400 mesh. After this treatment, the resultant powder was rubbed homogeneously onto Scotch tape, and the excess powder was removed. Furthermore, to avoid the sample thickness effect,[15,16] the condition $\Delta\mu x \leq 1$ must be satisfied, where $\Delta\mu x$ is the edge step. Therefore, the thickness of the samples was manipulated by folding the sample-coated Scotch tape to achieve $\Delta\mu x \sim 1$. The spectra were scanned from 8.75 to 10.25 keV using a gas-ionization detector. The ion chambers used for measuring the incident (I_0) and transmitted (I) synchrotron beam intensities were filled with a mixture of N_2 and He gases and a mixture of N_2 and Ar gases, respectively. Moreover, to ensure reliability of the spectra, the spectrum of Cu metal foil was also monitored to evaluate the stability of the energy scale for each measurement.

EXAFS Data Analysis. The data analysis for the experimental EXAFS spectra was performed using the UWXAFS package.[17,18] The AUTOBK[19] code was used for background subtraction. The criteria of good background should remove the optimization of the low-R portion of the EXAFS data, which was Fourier transformed to R-space. The normalized EXAFS spectrum obtained is

$$\chi(k) = \frac{\mu(k) - \mu_0(k)}{\Delta\mu 0(0)} \tag{1}$$

where $k = [2m(E - E_0)/\eta]^{1/2}$ is the wavenumber, E is the photon energy, E_0 is the threshold energy, $\mu(k)$ is the measured absorption coefficient, $\mu_0(k)$ is the background, and $\Delta\mu_0(0)$ is the edge jump. The resulting EXAFS spectra were k^3-weighted and Fourier transformed in the range $1.55 \leq k \leq 13.25$ Å^{-1} with a Hanning apodization function. A nonliner least-squares curve fitting procedure in the FEFFIT code[20] was carried out for the inverse Fourier transformation of $k^3\chi(k)$ to R-space, and fitting was done in the range $1.4 \leq R \leq 2.63$ Å, corresponding to the first shell of Cu−O.

Based on the plane wave single scattering, the general EXAFS formula[21,22] can be expressed as a summation over all shells i by the equation

$$\chi(k) = S_0^2 \sum_i \frac{N_i F_i(k)}{kR_i^2} \sin[2kR_i + \delta_i(k)] e^{-2R_i/\lambda} e^{-2k^2\sigma_i^2} \tag{2}$$

where $F_i(k)$ is the backscattering amplitude from each of the N_i atoms in the shell at distance R_i, with Debye−Waller factor σ_i^2. S_0 is the amplitude reduction factor, $\delta_i(k)$ is the total phase shift, and $\lambda(k)$ is the photoelectron mean free path. The values of $F_i(k)$, $\delta_i(k)$, and $\lambda(k)$ were calculated theoretically by a curved wave ab initio procedure in the code FEFF7.[23] The refinements were based on the minimization of R factor,[24] which is defined as follows:

$$R = \frac{\sum_{i=1}^{N} \{[\mathrm{Re}(f_i)]^2 + [\mathrm{Im}(f_i)]^2\}}{\sum_{i=1}^{N} \{[\mathrm{Re}(\tilde{\chi}_{\mathrm{data}\ i})]^2 + [\mathrm{Im}(\tilde{\chi}_{\mathrm{data}\ i})]^2\}} \tag{3}$$

where $f_i = \tilde{\chi}_{\mathrm{data}\ i} - \tilde{\chi}_{\mathrm{model}\ i}$ is the function to be minimized, $\tilde{\chi}$ is the χ function weighted by k^3, and N is the number of function evaluations. When fitting in R-space, $N = 2(R_{\max} - R_{\min})/\delta R$, where δR is the grid spacing in R-space.

On the basis of the X-ray powder diffraction pattern, we found that all samples from $x = 0.0$ and 1.0 have the same crystal structure type and space group. Thus, we use the crystal structure of $Bi_2Sr_2CaCu_2O_{8+\delta}$ determined from single-crystal X-ray diffraction data[25] as the reference model in EXAFS fitting. On the basis of the crystal structure, the first neighboring shell of Cu comprises five O atoms which construct a square pyramid. The distances are Cu−O(1) = 1.9126 Å and Cu−O(2) = 1.9148 Å in the Cu−O plane, and Cu−O(3) = 2.4993 Å in the apical direction. As the differences between the Cu−O(1) and Cu−O(2) distances are small, and therefore difficult to distinguish in EXAFS fitting, we set these two distances as a single refinable parameter ΔR_1. A common Debye−Waller factor (σ_e^2) was refined for these atoms. The Cu−O(3) distance and the corresponding Debye−Waller factor represented another two refinable parameters (ΔR_2 and σ_a^2). In the fitting procedure, only ΔE_0 (shift of the photoelectron energy origin), ΔR_1, ΔR_2, σ_e^2, and σ_a^2 were varied, and the coordination number N_i and S_0^2 were fixed. Here, $S_0^2 = 0.87$ was found from fitting the spectrum for the $x = 0.0$ sample, with the Cu−O distances on the Cu−O plane and the coordination number fixed on the basis of the values in the known crystal structure.

Results and Discussion

The powder X-ray diffraction patterns of the series of samples $Bi_2Sr_2(Ca_{1-x}Y_x)Cu_2O_{8+\delta}$ for $x = 0$ and 1 are shown in Figure 2. Each samples is a single phase. The powder X-ray diffraction patterns are interpreted on the basis of space group of *Bbmb*:1−11, with satellite reflections arising from an incommensurately modulated structure.[25,26] It is common to find the modulated structures in the Bi-based high-T_c cuprates due to the excess oxygen present in the Bi_2O_2 layers.[25,26] To assign the main peaks and satellite peaks, four integer indices, h, k, l, and m, are used. The c lattice parameter decreases monotonically from 30.8534(12) Å for $x = 0$ to 30.1766(11) Å for $x = 1$, corresponding to a 2.19% decrease. The a and b lattice parameters increase from

(14) Lu, K. Q.; Stern, E. A. *Nucl. Instrum. Methods* **1983**, *212*, 475.
(15) Lytle, F. W.; van der Laan, G.; Greegor, R. B.; Larson, E. M.; Violet, C. E.; Wong, J. *Phys. Rev. B* **1990**, *41*, 8955.
(16) Stern, E. A.; Kim, K. *Phys. Rev. B* **1981**, *23*, 3781.
(17) Frenkle, A. I.; Stern, E. A.; Voronel, A.; Qian, M.; Newville, M. *Phys. Rev. B* **1993**, *48*, 12449.
(18) Frenkle, A. I.; Stern, E. A.; Voronel, A.; Qian, M.; Newville, M. *Phys. Rev. B* **1994**, *49*, 11662.
(19) Newville, M.; Livins, P. Yacoby, Y.; Rehr, J. J.; Stern, E. A. *Phys. Rev. B* **1993**, *47*, 14126.
(20) Newville, M.; Ravel, B.; Haskel, D.; Rehr, J. J.; Stern, E. A. *Physica B* **1995**, *208*, 154.
(21) Sayers, D. E.; Bunker, B. A. In *X-ray Absorption: Principles, Applications, Techniques of EXAFS, SEXAFS, and XANES*; Koningsberger, DC; Prins, R., Eds; Wiley-Interscience: New York, 1988; pp 211−253.
(22) Stern, E. A. In *X-ray Absorption: Principles, Applications, Techniques of EXAFS, SEXAFS, and XANES*; Koningsberger, D. C.; Prins, R., Eds; Wiley-Interscience: New York, 1988; pp 3−51.
(23) Zabinsky, S. I.; Rehr, J. J.; Ankudinov, A.; Albers, R. C.; Eller, M. J. *Phys. Rev. B* **1995**, *52*, 2995.
(24) Newville, M. *FEFFIT Document* 1996.
(25) Petricet, V.; Gao, Y.; Lee, P.; Coppens, P. *Phys. Rev. B* **1990**, *42*, 387.
(26) Onoda, M.; Yamamoto, A.; Takayama-Muromachi E.; Takekakawa, S. *Jpn. J. Appl. Phys.* **1988**, *27*, L833.

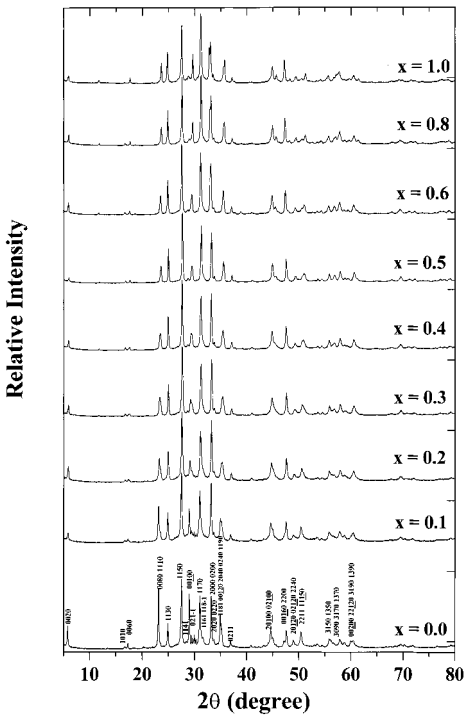

Figure 2. Powder X-ray diffraction patterns for the samples $Bi_2Sr_2(Ca_{1-x}Y_x)Cu_2O_{8+\delta}$ as a function of x.

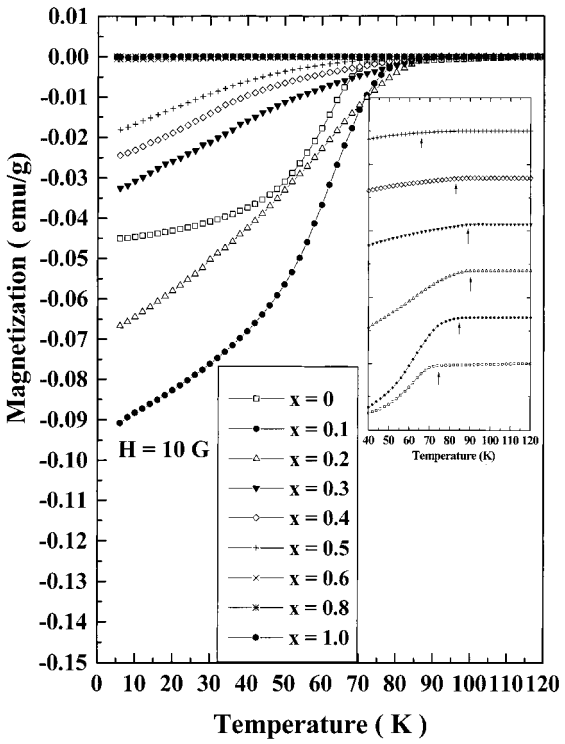

Figure 3. Temperature dependence of low-field (H = 10 G) magnetization of the $Bi_2Sr_2(Ca_{1-x}Y_x)Cu_2O_{8+\delta}$ samples.

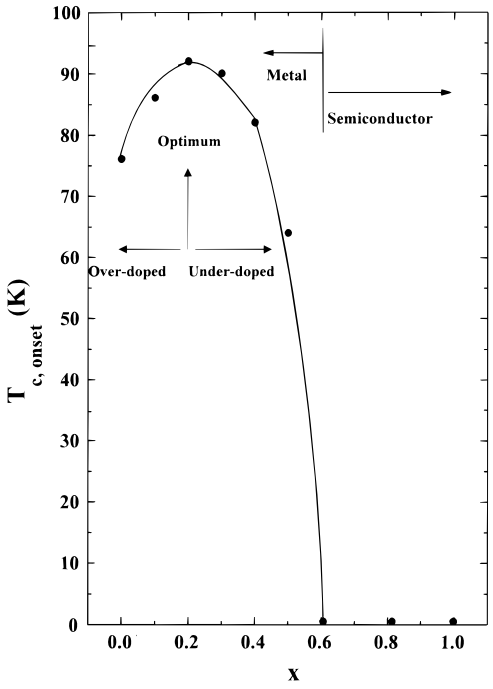

Figure 4. Value of T_c as a function of the compositional parameter x in $Bi_2Sr_2(Ca_{1-x}Y_x)Cu_2O_{8+\delta}$.

5.39828(19) and 5.40818(20) Å to 5.43782(19) and 5.44930(20) Å, representing increases of 0.83% and 0.76%, respectively. The contraction of c as x increases in $Bi_2Sr_2(Ca_{1-x}Y_x)Cu_2O_{8+\delta}$ is related to the fact that Y^{3+} [radius 1.019 Å for coordination number (CN) = 8] is smaller than Ca^{2+} (radius 1.12 Å for CN = 8).[27] We propose that the expansion along a and b as x increases may be attributed to a decrease in the nominal copper oxidation state, arising from the substitution of Y^{3+} for Ca^{2+}, which in turn leads to longer Cu−O distances within the sheets. The contraction of c and expansion of a and b as the Y content in $Bi_2Sr_2(Ca_{1-x}Y_x)Cu_2O_{8+\delta}$ increases may also be related to the response to "chemical pressure" in the system. Strain induced from the c axis due to the contraction may be released into the $a-b$ planes giving rise to expansion in these directions.

In Figure 3, we show the temperature dependence of low-field (H = 10 G) magnetization of the $Bi_2Sr_2(Ca_{1-x}Y_x)Cu_2O_{8+\delta}$ samples. The diamagnetic onset temperature (corresponding to superconducting transition temperature, T_c) of the $x = 0$ sample appears at around 75 K. The substitution of Ca^{2+} by Y^{3+} increases T_c up to 92 K for $x = 0.2$. However, for $x > 0.3$, T_c decreases again. We therefore propose that the substitution of high-valent Y^{3+} for low-valent Ca^{2+} in the system $Bi_2Sr_2(Ca_{1-x}Y_x)Cu_2O_{8+\delta}$ gives rise to a decrease in the hole concentration in the CuO_2 planes and increases T_c in the range $0 \le x \le 0.2$ via the addition of electrons from the $\sigma^*_{x^2-y^2}$ band.[28] Moreover, the samples with $0 \le x < 0.2$ exhibit overdoped holes. This proposal is partly supported by the observed expansion of the lattice parameters a and b as the Y doping increases. For $x > 0.2$, the value of T_c decreases due to the deficiency of holes within the CuO_2 planes. In Figure 4, we show T_c as a function of the compositional parameter x in $Bi_2Sr_2(Ca_{1-x}Y_x)Cu_2O_{8+\delta}$. This system has superconductivity over the composition range $x = 0-0.5$, with a maximum superconducting transition temperature of 92 K at $x = 0.2$. However, toward higher Y doping ($0.2 < x < 0.6$), the value of T_c decreases, leading to the dome-shaped curve shown in Figure 4. Moreover, across the composition range $x = 0.5-1.0$, the materials undergo a metal−insulator transition, assessed from our resistivity measurements. One attraction of this system is

(27) Shannon, R. D. *Acta Crystallogr. Sect. A* **1976**, *32*, 751.
(28) Goodenough, J. B. *Supercond. Sci. Technol.* **1990**, *3*, 26.

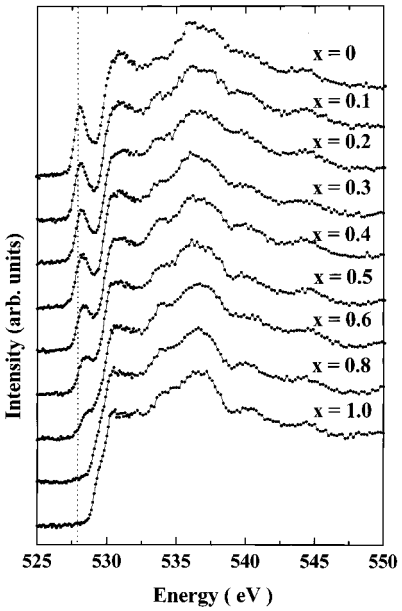

Figure 5. O K-edge XANES spectra for the series of $Bi_2Sr_2(Ca_{1-x}Y_x)Cu_2O_{8+\delta}$ samples with $x = 0-1.0$ in the energy range 525−555 eV, obtained with a bulk-sensitive total X-ray−fluorescence yield technique at room temperature.

that the hole concentration in the CuO_2 planes can be controlled by a simple chemical substitution involving other layers in the structure. Clearly, detailed studies of the electronic structure near the Fermi level using XANES and the local structure around the CuO_2 planes using EXAFS are of particular importance.

Figure 5 shows the O K-edge XANES spectra for the series of $Bi_2Sr_2(Ca_{1-x}Y_x)Cu_2O_{8+\delta}$ samples with $x = 0-1.0$ in the energy range 525−555 eV, obtained with a bulk-sensitive total X-ray−fluorescence yield technique. The O K-edge X-ray absorption spectrum for the sample with $x = 0$, as shown in Figure 5, mainly consists of a pre-edge around 528 eV and a broad peak above 530 eV. The pre-edge peak at ∼528.3 eV in Figure 5 can be ascribed to the transition from $3d^9L$ to $O1s3d^9$ (L denotes a hole in an $O2p_{x,y}$ orbital) states corresponding to creation of a core hole on the O 1s level and a filling of the $O2p_{x,y}$ states admixed to the upper Hubbard band.[10,11,29] The transition is strongly related to the variation of the hole concentration within the CuO_2 planes. The contribution of the broad peak above 530 eV is due to the wide antibonding $Bi6p_{x,y,z}-O$ and $O2p_{x,y}-O2P_z$ band. The pre-edge peaks were analyzed by fitting Gaussian functions. In Figure 6, the integrated intensity of the pre-edge peaks is plotted as a function of the compositional parameter x. Clearly, the intensity of the pre-edge peak at ∼528 eV, originating from the CuO_2 planes, decreases in intensity as the Y doping increases. This effect may indicate that the hole concentration within the CuO_2 planes decreases as the Y doping increases. Figure 7 shows that the absorption energy of the pre-edge peak at maximum intensity increases as the Y content (x) increases, demonstrating that the Fermi level moves to higher energy corresponding to a decrease in hole concentration within the CuO_2 planes.

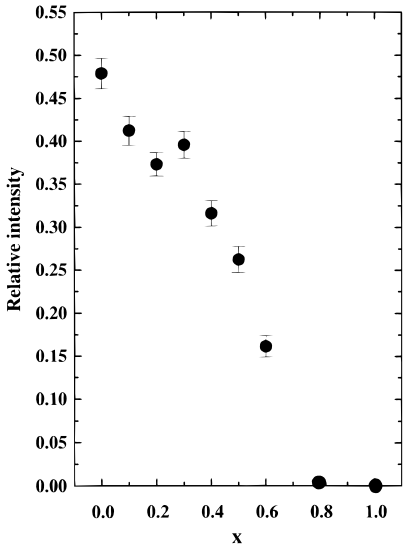

Figure 6. Integrated intensity of the pre-edge at ∼528.3 eV as a function of x in $Bi_2Sr_2(Ca_{1-x}Y_x)Cu_2O_{8+\delta}$.

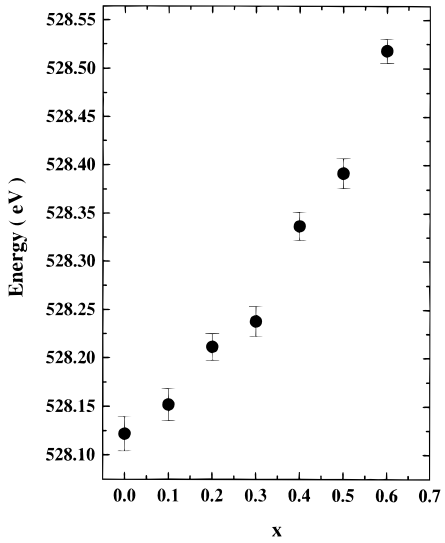

Figure 7. Onset absorption energy of the pre-edge peak as a function of x in $Bi_2Sr_2(Ca_{1-x}Y_x)Cu_2O_{8+\delta}$.

The unoccupied Cu 3d states can be probed by the Cu L-edge X-ray absorption spectrum, which exhibits strong excitonic character due to a significant overlap of the final 3d wave functions with those of the 2p core hole. The Cu L_{23}-edge X-ray absorption near edge structure total fluorescence yield spectra at room temperature in the energy range 920−960 eV are shown in Figure 8. For $x = 0.0$, the Cu L_{23}-edge absorption spectrum has two narrow peaks centered at 931.4 and 951.4 eV, respectively. In the Cu L_{23}-edge absorption spectrum of CuO, a white line at 931.2 eV and satellite structure at 937 eV are found corresponding to transitions to $(2p_{3/2})^{-1}3d^{10}$ and $(2p_{3/2})^{-1}3d^94s$ final states, respectively, where $(2p_{3/2})^{-1}$ denotes a $2p_{3/2}$ hole.[30] Therefore, the absorption peaks at 931.4 and 951.4 eV as shown in Figure 8 are ascribed to transitions from the $Cu(2p_{3/2,1/2})3d^9$-$O2p^6$ ground-state configuration (formal Cu^{2+} state) to the $Cu(2p_{3/2,1/2})^{-1}3d^{10}$-$O2p^6$ excited

(29) Fink, J.; Nücker, N.; Pellergin, E.; Romberg, H.; Alexander, M.; Knupfer, M. *J. Electron Spectrosc. Relat. Phenom.* **1994**, *395*, 66.

(30) Grioni, M.; Goedkoop, J. B.; Schoorl, R.; de Groot, F. M. F.; Fuggle, J. C.; Schafers, F.; Koch, E. E.; Rossi, G.; Esteva, J. M.; Karnatak, C. *Phys. Rev. B* **1989**, *39*, 1541.

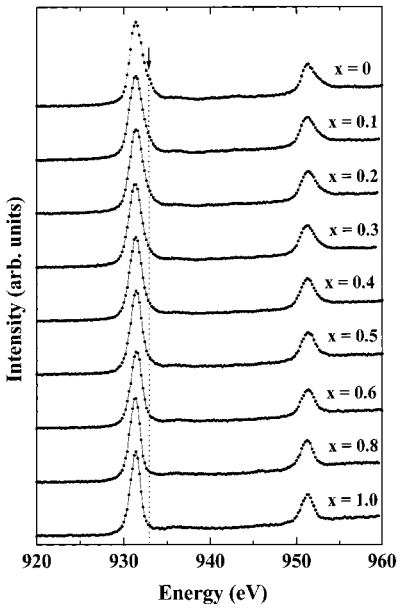

Figure 8. Cu L_{23}-edge X-ray absorption near-edge structure total fluorescence yield spectra of $Bi_2Sr_2(Ca_{1-x}Y_x)Cu_2O_{8+\delta}$ at room temperature in the energy range 920−960 eV. The arrow indicates the position of the defect states on the copper sites.

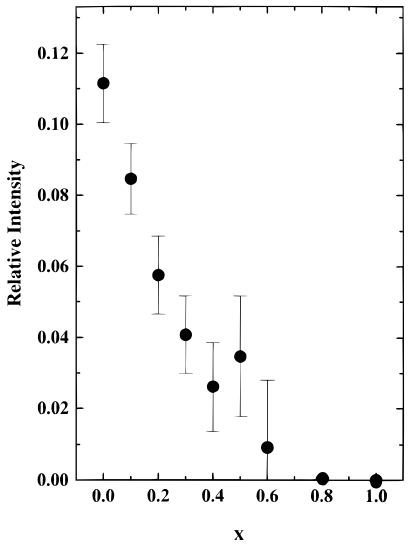

Figure 9. Dependence of the normalized intensity of the defect states on the copper sites (at 932.9 eV) as a function of the compositional parameter x in $Bi_2Sr_2(Ca_{1-x}Y_x)Cu_2O_{8+\delta}$.

state. Moreover, two new features are apparent at the high-energy side of the main absorption peaks of the $x = 0$ sample, causing asymmetry of the absorption peaks. For samples with increasing x (i.e., decreasing hole concentration), the absorption peaks become more symmetric. From the curve-fitting, the new features are found to be centered at 932.9 and 952.9 eV, respectively. In Figure 9, the area under this high energy shoulder, estimated by fitting the main peak and the shoulder by Gaussian functions, is plotted as a function of the compositional parameter x. As seen from Figure 9, the normalized intensity of this high-energy shoulder decreases as the Y concentration increases.

We note that the curve in Figure 9 resembles the behavior of the pre-edge peak at ∼ 528.3 eV in the O K-edge absorption spectra shown in Figure 6. It may then be suggested that these high-energy features could

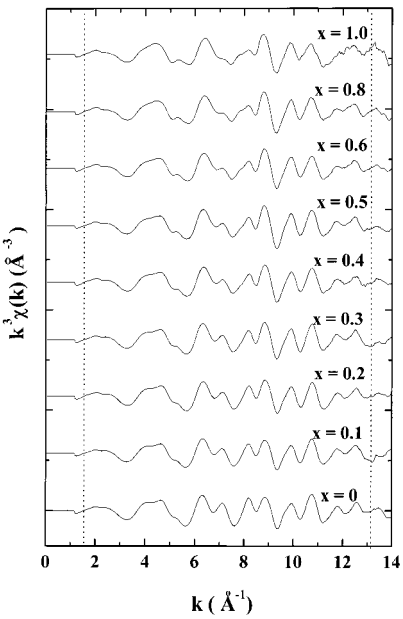

Figure 10. Experimental k^3-weighted Cu K-edge EXAFS spectra of $Bi_2Sr_2(Ca_{1-x}Y_x)Cu_2O_{8+\delta}$.

originate from the O 2p hole states and could be assigned as transitions from the $Cu(2p_{3/2,1/2})3d^9L$ ground state (formal Cu^{3+} state) to the $Cu(2p_{3/2,1/2})^{-1}3d^{10}L$ excited state, where L denotes the O 2p ligand hole.[31,32] As the Y concentration increases, the 2p holes on the oxygen sites decrease (corresponding to the $Cu3d^9L$ defect state), leading to a decrease in the intensity of the high-energy shoulder in the Cu L-edge absorption spectra. Similar to the defect states in O 1*s* XANES spectra, these electronic states disappear on reducing the sample and transforming to the semiconducting or insulating state. Because there is only one type of Cu site in the asymmetric unit of $Bi_2Sr_2(Ca_{1-x}Y_x)Cu_2O_{8+\delta}$ (i.e., there are no Cu−O chains as in $YBa_2Cu_3O_{7-\delta}$), these high-energy features in the Cu L-edge absorption spectra can be identified as the result of the hole doping in the O sites within the CuO_2 layers due to the chemical substitution of Y^{3+} for Ca^{2+}. The close resemblance between the high-energy features in the Cu L-edge absorption spectra and the pre-edge peak at 528.3 eV in the O 1s absorption spectra gives evidence in support of the suggestion that the pre-edge peak at 528.3 eV originates from the O(1) and O(2) sites within the CuO_2 planes.

Experimental k^3-weighted Cu K-edge EXAFS spectra of $Bi_2Sr_2(Ca_{1-x}Y_x)Cu_2O_{8+\delta}$ are shown in Figure 10, and the Fourier transforms $\{|\tilde{\chi}(R)| = FT[k^3\chi(k)]\}$ are shown in Figure 11. The solid lines and empty circles represent the fitted and experimental data, respectively. The first prominent peak (I) in the Fourier transform is assigned to the equatorial (in-plane) and axial (out-of-plane) Cu−O distances (as discussed above), and is followed by the second peak (II) corresponding to the Cu−Ca and Cu−Sr distances. The third prominent peak (III) is assigned to the Cu−Cu distance. Our research is focused

(31) Bianconi, A.; Congiu Castellano, A.; de Santis, M.; Rudolf. P.; Lagarde, P.; Flank, A. M.; Marcelli, A. *Solid State Commun.* **1987**, *63*, 1009.
(32) Sarma, D. D.; Strebel, O.; Simmons, C. T.; Neukirch, U.; Kaindl, G. *Phys. Rev. B* **1988**, *36*, 8285.

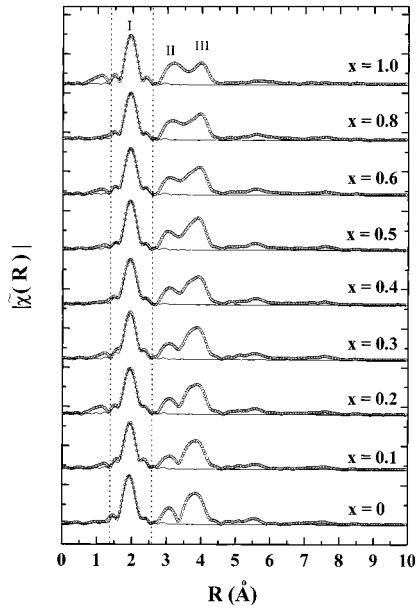

Figure 11. Fourier transforms $\{|\tilde{\chi}(R)| = FT[k^3\chi(k)]\}$ of the Cu K-edge EXAFS spectra of $Bi_2Sr_2(Ca_{1-x}Y_x)Cu_2O_{8+\delta}$.

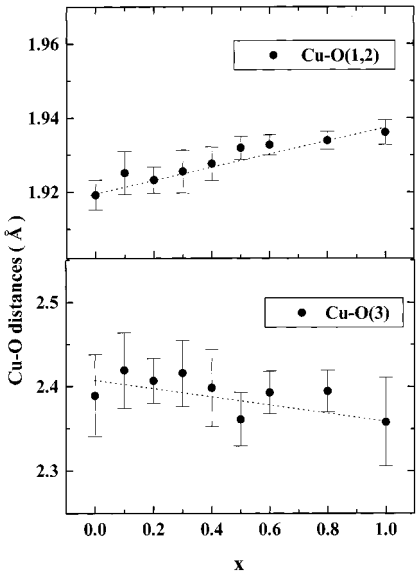

Figure 12. (a) Equatorial Cu−O(1,2) bond distances and (b) axial Cu−O(3) bond distances, in $Bi_2Sr_2(Ca_{1-x}Y_x)Cu_2O_{8+\delta}$ samples as a function of the compositional parameter *x*.

on the variation of the local structure of the CuO_5 square pyramidal arrangement, and we therefore only discuss the fitting on the first peak (I) in order to obtain the Cu−O bond distances. The variation of the equatorial Cu−O(1,2) bond lengths as a function of the compositional parameter *x* is shown in Figure 12(a). As *x* increases, the equatorial Cu−O bond distance is found to increase, and is consistent with the variation of the lattice parameters *a* and *b* on increasing x. The variation of the axial Cu−O(3) bond distance as a function of the compositional parameter *x* is shown in Figure 12(b). The axial Cu−O bond distance is found to decrease as *x* increases, reflecting the variation of the lattice parameter *c*. According to the XANES results, the hole concentration within the CuO_2 planes decreases as the Y content increases, giving rise to an increase in electron density in the antibonding state. Thus, the bond order of Cu−O(1,2) in the CuO_2 planes should decrease as the Y content increases. This effect may result in an increase in the Cu−O(1,2) bond lengths, consistent with our observations from the analysis of the EXAFS data.

Concluding Remarks

The chemical substitution of Y^{3+} for Ca^{2+} in $Bi_2Sr_2(Ca_{1-x}Y_x)Cu_2O_{8+\delta}$ may be similar to the application of "chemical pressure" in the parent $Bi_2Sr_2CaCu_2O_{8+\delta}$ system, leading to a contraction of the *c* lattice parameter and expansion of the *a* and *b* lattice parameters. Near the O 1s edge, the pre-edge peak at ~528.3 eV is ascribed to the core-level excitations of O 1s electrons to O 2p hole states located in the CuO_2 planes. The intensity of this pre-edge peak decreases as the Y doping increases, demonstrating that the chemical substitution of Y^{3+} for Ca^{2+} in $Bi_2Sr_2(Ca_{1-x}Y_x)Cu_2O_{8+\delta}$ gives rise to a decrease in hole concentrations within the CuO_2 planes. The intensity of this pre-edge peak closely correlates with the variation of the superconducting transition temperature with compositions, showing that holes generated in the O 2p orbitals within the CuO_2 planes play an important role in controlling the value of T_c in these systems. The results from the Cu L-edge X-ray absorption spectra are consistent with those from O 1s X-ray absorption spectra. Our EXAFS results confirm that the variation of the local structure of the CuO_5 pyramids (expansion of the equatorial Cu−O bond distance and contraction of the axial Cu−O bond distance as the Y content increases) is consistent with the change in periodicity (long-range structural properties) as determined by XRD. Therefore, structural changes due to substitution of Y^{3+} for Ca^{2+} in $Bi_2Sr_2(Ca_{1-x}Y_x)Cu_2O_{8+\delta}$ correspond to O(3) moving toward the CuO_2 planes with expansion of the Cu−O(1) and Cu−O(2) bond distances. These structural changes are associated with a decrease in hole concentration within the CuO_2 planes, affecting the superconductivity.

Acknowledgment. We thank Dr. M. Newville (Argonne National Lab), Dr. B. Ravel (National Institute of Standards and Technology), and Prof. P. W. Stephens (Stony Brook State University of New York) for useful discussions. This research was supported financially by the National Science Council of the Republic of China under Grant Number NSC88-2113-M-002-029.

CM9907007